International Journal of Solids and Structures 51 (2014) 894–903

Contents lists available at ScienceDirect

International Journal of Solids and Structures

journal homepage: www.elsevier.com/locate/ijsolstr

Nonlinear delamination buckling and expansion of functionally graded laminated piezoelectric composite shells

W.D. Yang [a], W. Zhang [a,b], X. Wang [a,*], G. Lu [b]

[a] School of Naval Architecture, Ocean and Civil Engineering (State Key Laboratory of Ocean Engineering), Shanghai Jiaotong University, Shanghai 200240, PR China
[b] School of Mechanical and Aerospace Engineering, Nanyang Technological University, Singapore

ARTICLE INFO

Article history:
Received 14 June 2013
Received in revised form 16 November 2013
Available online 27 November 2013

Keywords:
Functionally graded composite shells
Piezoelectric layer
Delaminated buckling
Electric field
Thermal loading

ABSTRACT

In this paper, an analytical method is presented to investigate the nonlinear buckling and expansion behaviors of local delaminations near the surface of functionally graded laminated piezoelectric composite shells subjected to the thermal, electrical and mechanical loads, where the mid-plane nonlinear geometrical relation of delaminations is considered. In examples, the effects of thermal loading, electric field strength, the stacking patterns of functionally graded laminated piezoelectric composite shells and the patterns of delaminations on the critical axial loading of locally delaminated buckling are described and discussed. Finally, the possible growth directions of local buckling for delaminated sub-shells are described by calculating the expanding forces along the length and short axis of the delaminated sub-shells.

1. Introduction

Functionally graded material (FGM) is microscopically inhomogeneous composites composed of some different materials along a determined direction (Reddy, 2000; Shen, 2005; Shariyat, 2009a). By gradually changing the volume fraction of constituent materials, the properties of FGM appear in a smooth and continuous variation from one surface to another, so that the interface stress concentration usually taking place in laminated composite structures can be eliminated. Therefore, FGM have been potential for the engineering application for tailoring the desired thermo-mechanical properties. Piezoelectric materials are widely utilized in modern engineering due to its direct and inverse electro-mechanical effects (Shariyat, 2008, 2009b). Investigations on the usage of piezoelectric layer in active structure control as noise attenuation, deformation control and vibration suppression have been presented. As the usage of these materials increases, the composite structures consist of the fiber reinforced layer, piezoelectric material layer and FGM layer have been the focus in the engineering application of smart structure. Thus, it is important to understand the deformation and failure characteristics of FGM laminated piezoelectric composite structures under various loads (Sheng and Wang, 2011, 2009a,b; Sarangi and Ray, 2013).

Numerous studies on the FGM and piezoelectric material structures subjected to mechanical, thermal and electrical loads have been performed. Assuming that the material property of the FGM beam was graded in the thickness direction according to a simple exponent-law distribution, a thermo-elastic solution of FGM hybrid beam with simply-supported edges under pressure and thermal loads was presented (Alibeigloo, 2010; Alibeigloo and Chen, 2010). Shen (2009) investigated the compressive postbuckling of shear deformable functionally graded piezoelectric plate under thermal loading. Malekzadeh et al. (2012) presented the dynamical analysis of pressurized rotating multi-layered FGM cylindrical shells in thermal environment, in which the variations of the field variables across the shell thickness were described by dividing the shell into a set of layers along the radial direction. Wu (2007) investigated the deformation characteristics of functionally graded laminated piezoelectric cylindrical shells subjected to coupling bend and electromechanical loads utilizing the perturbation method. Based on Fourier differential quadrature and polynomial differential quadrature methods, Alashti and Khorasnd (2011) described three-dimensional thermo-elastic analytical method of a FGM cylindrical shell with piezoelectric layers under the asymmetric thermo-electro-mechanical loads. Sheng and Wang (2010) investigated the coupling thermopiezoelectric elastic problem of FGM laminated composite shells subjected to moving mechanical loads and sudden temperature change, where active vibration was controlled by using piezoelectric layers embedded on the surface of functionally graded shell.

Because of the manufacturing defects and the surface damages induced by impact with lower energy, the local delamination near the surface of laminated structures is one of main failure modes, so that the delamination failure along the interface of laminated structures has been concerned in the optical

* Corresponding author. Tel./fax: +86 021 54745367.
E-mail address: xwang@sjtu.edu.cn (X. Wang).

0020-7683/$ - see front matter © 2013 Elsevier Ltd. All rights reserved.
http://dx.doi.org/10.1016/j.ijsolstr.2013.11.017

design of composite laminated structure. Ghasemnejad et al. (2010) investigated the effect of hybrid laminate lay-up with different delamination positions in composite laminated beam. Predicting the damage and expanding extents of delaminations is essential to the continued employment of laminated composite structures in various engineering applications. Naghipour et al. (2011) studied the delamination mode in multidirectional laminate structures subjected to fatigue loading by simulating and experimental methods.

Because laminated composite structures are often subjected to loading in-plane, delaminated sub-structures easily appear in local buckling. Therefore, the delaminated buckling of laminated composite structures under various loads is one of the most critical problems in composites engineering application and is much attended. Delaminations (sub-laminations) near the surface of laminated structures are much smaller than the layer number of laminated structures (base-laminations), so that the deformation of delaminations is free and the boundary of the local delamination is fixed at the interface between sub-lamination and base-lamination. In previous literature, many investigations on the delaminated buckling of laminated composite structures have mainly focused on the delaminated buckling of fiber reinforced laminated structures. Tsouvalis and Garganidis (2011) described the effect of some delamination parameters on the delaminated buckling characteristics of laminated composite structures. Based on the modified variational principle and a nonlinear spring-layer model, Li (2012) presented a three-dimensional analytical model to study delaminated buckling for laminated composite cylindrical shells. Chirica and Beznea (2012) described the effect of delaminations on the buckling and postbuckling characteristics of the laminated composite plates subjected to shear and compression loadings. Obdržáleka and Vrbkab (2011) investigated the buckling and postbuckling behavior of delaminations in laminated composite plates with irregularly delaminated shapes. Based on laminated plate theories, Kharazi et al. (2010) presented an analytical method to study the delaminated buckling behavior of the composite laminates with through-the-width delaminations. Craven et al.(2010) investigated delaminated buckling for a carbon fibre composite laminate with multiple delaminations of realistic shape subjected to compression loading by utilizing a finite element model. Tay (2003) gave an overview on characterization and analysis of delamination fracture in laminated composite structures. Ren (2008) presented an investigation into the buckling of orthotropic piezoelectric rectangular laminates with weak interfaces based on the state-space formulation established directly from the three-dimensional theory of elasticity. Bruno and Greco (2000) gave a continuous analysis method to calculate one-dimensional modeling of failure in laminated beams and plates. Meng et al. (2010) reported the result of an investigation into the buckling characteristics for the local delamination near the surface of piezoelectric laminated shells, where local delaminated sub-shells may be monolayer and multiplayer. However, investigations on buckling behaviors of local delaminated sub-shells near the surface of FGM-laminated piezoelectric composite shells under thermal, electrical and axial compressed loads have not presented in literatures because of its complexity.

In this paper, an analytical method is presented to investigate the nonlinear buckling characteristics for local delamination near the surface of FGM laminated piezoelectric composite shells subjected to coupling electric, thermal and mechanical loads, where FGM laminated piezoelectric composite shells consist of FGM layers, piezoelectric layers and carbon fiber reinforced layers and the stack sequence of delaminated patterns near the surface of FGM laminated piezoelectric composite shells is arbitrary. The nonlinear temperature distribution along the thickness of FGM is given by solving the thermal conductive equation of FGM shell. The piezoelectric layers bonding the internal and external surface of FGM laminated piezoelectric composite shells are taken as active control layer by radial polarizing. The carbon fiber layer in FGM laminated piezoelectric composite shells is used to enhance the strength and stiffness of the FGM laminated piezoelectric composite shells. The material properties of carbon fiber layer and piezoelectric layer are taken as a function of temperature change. In examples, the stacking patterns of FGM laminated piezoelectric composite shells are, respectively, taken as $[P_0/30°/60/90/\mathrm{FGM}/90°/60/30/P_0]$ and $[P_0/0°/45°/-45°/\mathrm{FGM}/-45°/45°/0°/P_0]$, in which P_0 represents piezoelectric layer, and the other layers present fiber reinforced layers. The stacking patterns of locally delaminated sub-shells are $[P_0]$, $[P_0/30°]$ and $[P_0/0°]$. The results show the effects of thermal loading, electric field, stacking pattern and delaminated pattern on the critical loading of locally nonlinear delaminated buckling. Finally, by calculating the expanding forces along the length and short axis of elliptical delaminations, the possibly expanding directions of locally nonlinear buckling for the elliptical delaminations are described and discussed.

2. Calculating model and basic equations

Fig. 1 shows that a FGM (Functionally Graded Material) laminated piezoelectric composite shells is composed of FGM layer, fiber reinforced layers and piezoelectric layers, where the fiber layer and piezoelectric layer embedded on inner and outer surfaces of the FGM laminated piezoelectric composite shells is acted as reinforced and actuator effects. When the surface of FGM laminated piezoelectric composite shells is impacted by objects, a local delamination with arbitrary sequence may occur near the surface of the FGM-laminated piezoelectric shells. Because FGM layer is a single layer and the piezoelectric fiber reinforced layers is symmetrical to the FGM layer, only the tension and bending coupling effect of locally delaminated sub-shells is considered in the present model. Here, R, h_b and h_s, respectively represent the mid-plane radius, the thickness of FGM laminated piezoelectric shells and the thickness of delaminations, where $h_b/R \ll 1$ and $h_s/h_b \ll 1$. The axial, circumferential and radial directions of FGM-laminated piezoelectric shells are denoted by global coordinate system (x, y, z) fixed at the mid-plane of FGM-laminated piezoelectric shells. The geometric axes of delaminations are denoted by the local coordinate system (x', y', z') fixed at the mid-plane of delaminated sub-shells. The angle between the axes x and x' in two coordinate systems is defined as φ. The material's main axes of the fiber reinforce and piezoelectric active layers are defined by $(1, 2, 3)$, and the angle between the material's main axes 1–2 and the global coordinate axis x–y is defined by θ.

The material property of FGM layer is described using a simple rule of mixtures composed of metal and ceramic (Fig. 1), and varies along the thickness of FGM layer according to a power low, as follows:

$$F_{eff}(z) = F_o V(z) + F_i(1 - V(z)), \quad V(z) = \left(\frac{z + h_f/2}{h_f}\right)^{\Phi}, \quad -0.5h_f \leqslant z \leqslant 0.5h_f \tag{1}$$

where F_{eff} is used to effectively describe the variation of elastic modulus, mass density, Poisson's ratio, thermal expansion coefficient and the thermal conductivity of functionally graded materials along the thickness h_f of FGM layer, F_o and F_i denote the material property of the outer surface $(z = 0.5h_f)$ and inner surface $(z = -0.5h_f)$ of the FGM layer, respectively, and Φ denotes the volume fraction exponent $(\Phi \geqslant 0)$.

Expanding Eq. (1), the effective elastic modulus, thermal expansion coefficient and thermal conductivity of FGM layer are written as

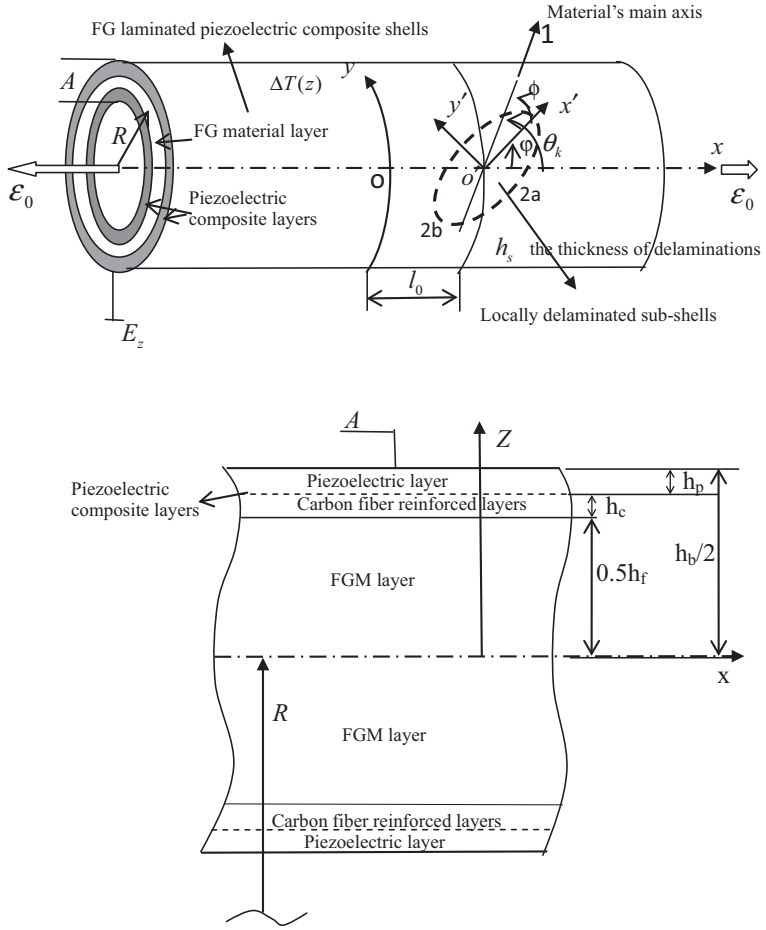

Fig. 1. Calculation models and coordinate systems of FGM laminated piezoelectric composite shells with local surface delamination.

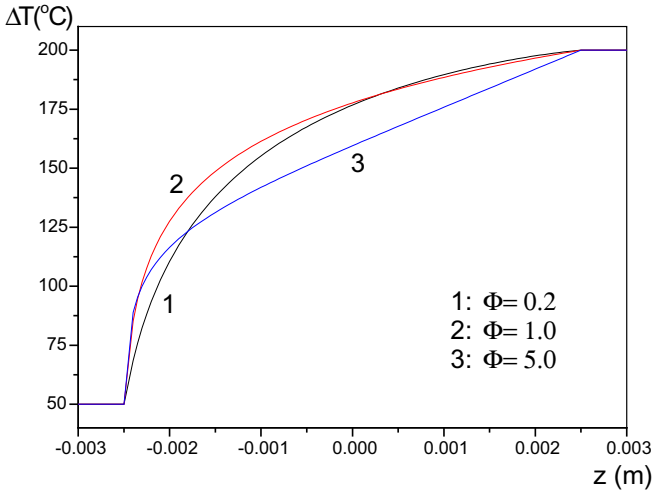

Fig. 2. Temperature distributions along the thickness of FGM laminated piezoelectric composite shells [P_0/30°/60°/90°/FGM/90°/60°/30°/P_0], where Φ expresses the volume fraction exponent of FGM layer, $\Delta T_i = 50\ ^\circ C$, $\Delta T_0 = 200\ ^\circ C$.

$$E_{eff} = (E_c - E_m)\left(\frac{z+0.5h_f}{h_f}\right)^{\Phi} + E_m, \quad \alpha_{eff} = (\alpha_c - \alpha_m)\left(\frac{z+0.5h_f}{h_f}\right)^{\Phi} + \alpha_m,$$
$$\kappa_{eff} = (\kappa_c - \kappa_m)\left(\frac{z+0.5h_f}{h_f}\right)^{\Phi} + \kappa_m, \quad -0.5h_f \leqslant z \leqslant 0.5h_f \tag{2}$$

where Poission's ratio v_{eff} of FGM layer depending weakly on temperature change is taken as a constant.

It is clear that the temperature distribution along the thickness of functionally graded laminated structures is dependent on different thermal boundaries and interface conditions between two layers, for example when the pertinent boundary conditions is taken from reference Alibeigloo (2011), the actual temperature distribution along the thickness of functionally graded shell with piezoelectric layers is in the form of Bessel function. However, in the present model, due to the thickness of piezoelectric composite layers is much smaller than that of FGM layer, only the thermal conduction effect of FGM layer is considered as shown in Fig. 2, and the temperature change along the thickness of piezoelectric composite layers is assumed as uniform distribution, which is well agreement with the practical fact.

The temperature field along the thickness of FGM layer is written as

$$T(z) = T_c - \frac{T_{cm}}{\int_{-0.5h_f}^{0.5h_f} dz/\kappa_{eff}(z)} \int_{-0.5h_f}^{z} \frac{dz}{\kappa_{eff}(z)}, \quad -0.5h_f \leqslant z \leqslant 0.5h_f \tag{3}$$

$$T_c = T_i = T(-0.5h_f), \quad T_m = T_o = T(0.5h_f) \tag{4}$$

where $T_{cm} = T_c - T_m$ is the temperature difference between the inner surface and the outer surface of the FGM layer.

Considering the temperature effects and assuming that the piezoelectric layer is polarized along the radial direction, the physical relation for the k layer of FGM laminated piezoelectric composite shells is written as

$$\begin{Bmatrix}\sigma_1\\ \sigma_2\\ \tau_{12}\end{Bmatrix}=\begin{bmatrix}Q_{11}^k & Q_{12}^k & 0\\ Q_{21}^k & Q_{22}^k & 0\\ 0 & 0 & Q_{66}^k\end{bmatrix}\left(\begin{Bmatrix}\varepsilon_1\\ \varepsilon_2\\ \gamma_{12}\end{Bmatrix}-\begin{Bmatrix}\alpha_1^k\\ \alpha_2^k\\ 0\end{Bmatrix}\Delta T_k-\begin{Bmatrix}d_1^k\\ d_2^k\\ 0\end{Bmatrix}E_z\right) \tag{5}$$

$$\begin{Bmatrix}D_1\\ D_2\\ D_3\end{Bmatrix}=\left(\begin{bmatrix}Q_{11}^k & Q_{12}^k & 0\\ Q_{12}^k & Q_{22}^k & 0\\ 0 & 0 & 0\end{bmatrix}\begin{bmatrix}0 & 0 & d_1^k\\ 0 & 0 & d_2^k\\ 0 & 0 & 0\end{bmatrix}\right)^T\begin{Bmatrix}\varepsilon_1\\ \varepsilon_2\\ \gamma_{12}\end{Bmatrix}-\begin{Bmatrix}p_1^k\\ p_2^k\\ p_3^k\end{Bmatrix}\Delta T_k-\begin{Bmatrix}q_1\\ q_2\\ q_3\end{Bmatrix}E_z \tag{6}$$

where $\Delta T_k = T(z)$ is the temperature change along the thickness of FGM laminated piezoelectric composite shells, $[Q_{ij}]$, $\{\alpha_i\}$, $\{d_i\}$, $\{F_i\}$, $\{p_i\}$, $\{q_i\}$ and E_z express the stiffness coefficient, thermal expansion coefficient, piezoelectric coefficient, electric displacement, pyroelectric coefficient, permittivity coefficient, and the electric field strength along the z direction, respectively.

The material proprieties of FGM layer ($-0.5h_f \leqslant z \leqslant 0.5h_f$) is inhomogeneous isotropic, as follows:

$$\begin{aligned}&Q_{11}^k=\tfrac{E_{eff}}{1-\nu_{eff}^2},\quad Q_{12}^k=\tfrac{\nu_{eff}E_{eff}}{1-\nu_{eff}^2}=Q_{21}^k,\quad Q_{22}^k=\tfrac{E_{eff}}{1-\nu_{eff}^2},\quad Q_{66}^k=\tfrac{E_{eff}}{2(1+\nu_{eff})}\\ &\alpha_1^k=\alpha_2^k=\alpha_{eff}(z),\quad \{d_i\}=\{p_i\}=\{q_i\}=E_z=0\end{aligned} \tag{7}$$

The material proprieties of fiber reinforced layer ($0.5h_f \leqslant |z| \leqslant 0.5h_b$) are given by

$$\begin{aligned}&Q_{11}^k=\tfrac{E_1}{1-\nu_{12}^2},\quad Q_{12}^k=\tfrac{\nu_{12}E_1}{1-\nu_{12}^2}=Q_{21}^k,\quad Q_{22}^k=\tfrac{E_2}{1-\nu_{12}^2},\quad Q_{66}^k=G_{12}\\ &\alpha_1^i=\alpha_1,\quad \alpha_2^i=\alpha_2,\quad \{d_i\}=\{p_i\}=\{q_i\}=E_z=0\end{aligned} \tag{8}$$

where subscripts 1 and 2 express the elastic constants and thermal expansion coefficients of material's main directions 1–2, respectively.

For piezoelectric layer ($0.5h_f \leqslant |z| \leqslant 0.5h_b$), $\{d_i\}$, $\{p_i\}$, $\{q_i\}$ and E_z are nonzero value.

The mid-plane displacements of FGM laminated piezoelectric composite shells along the global coordinate system x, y, z are denoted by u, v, w, respectively. For an axial symmetric problem, the mid-plane strains of FGM laminated piezoelectric composite shells in the global coordinate system (x, y, z) are expressed as

$$\varepsilon_x^0=\frac{du}{dx},\quad \gamma_{xy}^0=\frac{dv}{dx},\quad \varepsilon_y^0=\frac{2\pi(R-w)-2\pi R}{2\pi R}=-\frac{w}{R} \tag{9}$$

The relationship between the membrane force and the strain in the mid-plane of FGM laminated piezoelectric composite shells subjected to thermal loading and electric loading is written as

$$\begin{Bmatrix}N_x\\ N_y\\ N_{xy}\end{Bmatrix}=\begin{bmatrix}A_{11} & A_{12} & A_{16}\\ A_{12} & A_{22} & A_{26}\\ A_{16} & A_{26} & A_{66}\end{bmatrix}\begin{Bmatrix}\varepsilon_x\\ \varepsilon_y\\ \gamma_{xy}\end{Bmatrix}-\begin{Bmatrix}N_x^T\\ N_y^T\\ N_{xy}^T\end{Bmatrix}-\begin{Bmatrix}N_x^E\\ N_y^E\\ N_{xy}^E\end{Bmatrix} \tag{10}$$

where $[A_{ij}]$ represents the tensional stiffness of mid-plane of FGM laminated piezoelectric composite shells, N_x, N_y and N_{xy} represents the membrane forces of the mid-plane, $\{N_i^T\}$ represents the membrane force induced by thermal loading and $\{N_i^E\}$ represents the membrane force induced by the electric loading.

It is well known that the loading forms of axial edge tractions and edge moment exerted on the ends of shell structures are, generally, used to study the global buckling characteristics of intact FGM laminated shells. However, the local buckling for delaminated sub-shells in FGM laminated piezoelectric base-shells is mainly induced by axial loading. To simplify the complex process solving locally delaminated buckling near the surface of functionally graded laminated piezoelectric shells, the axial strain as a practical displacement loading is considered in the present model.

From Eqs. (9) and (10), the displacements u, v and w of FGM laminated piezoelectric composite shells only under an axial loading ε_0 are given by

$$u=\varepsilon_0 x,\quad v=(b_3\varepsilon_0+b_4)x,\quad w=-Rb_1\varepsilon_0-Rb_2 \tag{11}$$

The corresponding strain field of mid-plane is written as

$$\varepsilon_x=\varepsilon_0,\quad \varepsilon_y=b_1\varepsilon_0+b_2,\quad \gamma_{xy}=b_3\varepsilon_0+b_4 \tag{12}$$

where

$$\begin{aligned}&b_1=\tfrac{A_{16}A_{26}-A_{12}A_{66}}{A_{22}A_{66}-A_{26}^2},\quad b_2=\tfrac{A_{66}(N_y^T+N_y^E)-A_{26}(N_{xy}^T+N_{xy}^E)}{A_{22}A_{66}-A_{26}^2}\\ &b_3=\tfrac{A_{12}A_{26}-A_{16}A_{22}}{A_{22}A_{66}-A_{26}^2},\quad b_4=\tfrac{A_{22}(N_{xy}^T+N_{xy}^E)-A_{26}(N_y^T+N_y^E)}{A_{22}A_{66}-A_{26}^2}\end{aligned} \tag{12a}$$

In Eq. (10), the membrane forces induced by thermal and electric loads are, respectively, written as

$$\{N_i^T\}=\sum_{k=1}^{p}\int_{z_{k-1}}^{z_k}[\bar{Q}_{ij}]_k\{\bar{\alpha}_i\}_k\Delta T_k dz,\quad i=x,y,xy \tag{13a}$$

$$\{N_i^E\}=\sum_{k=1}^{p}\int_{z_{k-1}}^{z_k}[\bar{Q}_{ij}]_k\{\bar{d}_i\}_k E_z dz,\quad i=x,y,xy \tag{13b}$$

where ΔT_k and E_z represent, respectively, the temperature change and the electric field strength of the kth layer, $\{\bar{\alpha}_i\}_k$, $\{\bar{d}_i\}_k$ and $[\bar{Q}_{ij}]_k$ represent, respectively, the thermal expansion coefficient, piezoelectric coefficient and stiffness matrix of the kth layer in the global coordinate system (x, y, z), as follows:

$$\begin{aligned}&\{\bar{\alpha}_i\}_k=[T(\theta_k)]_\varepsilon\{\alpha_i\},\quad \{\bar{d}_i\}_k=[T(\theta_k)]_\varepsilon\{d_i\},\\ &[\bar{Q}_{ij}]_k=[T(\theta_k)]_\sigma[Q_{ij}][T(\theta_k)]_\sigma^T\end{aligned} \tag{13c}$$

where $\{\alpha_i\}$ and $\{d_i\}[Q_{ij}]$ are, respectively, the thermal expansion coefficient, piezoelectric coefficient and the stiffness matrix in the material's main axis (1–2). $[T(\theta_k)]_\sigma$ and $[T(\theta_k)]_\varepsilon$ express, respectively, the stress transformation matrix and strain transformation matrix, and is detailedly described in Appendix A.

As shown in Fig. 1, because the distance between origins of global coordinate system and local coordinate system is taken as l_0, any point $p(x, y)$ in global coordinate system (x, y) can be described by a local coordinate system (x', y'), as follows

$$x=l_0+x'\cos\varphi-y'\sin\varphi,\quad y=x'\sin\varphi+y'\cos\varphi \tag{14}$$

Utilizing the translation between two coordinate systems, the displacement components of FGM laminated piezoelectric composite shells in the local coordinate system are expressed as

$$\begin{aligned}u'&=[x'\cos^2\varphi+(nx'-y')\sin\varphi\cos\varphi-ny'\sin^2\varphi]\varepsilon_0+l_0\cos\varphi\varepsilon_0\\ &\quad+nl_0\sin\varphi\varepsilon_0+l_0d\sin\varphi+x'd\sin\varphi\cos\varphi-y'd\sin^2\varphi\\ v'&=[nx'\cos^2\varphi-(ny'+x')\sin\varphi\cos\varphi+y'\sin^2\varphi]\varepsilon_0\\ &\quad+nl_0\cos\varphi\varepsilon_0-l_0\varepsilon_0\sin\varphi+l_0d\cos\varphi+x'd\cos^2\varphi-y'd\sin\varphi\cos\varphi\\ w'&=-Rm\varepsilon_0-Rc\end{aligned} \tag{15}$$

The displacements of delaminations in the local coordinate axes are denoted by u'', v'', w''. Considering that the mid-plane radius of delaminations satisfies $R' >> w''$, the mid-plane strain, curvature and twist curvature of delaminations based on a nonlinear shallow shell theory is expressed as

$$\begin{aligned}&\varepsilon_{x'}=\tfrac{\partial u''}{\partial x'}-\tfrac{w''}{R}\sin\varphi+\tfrac{1}{2}\left(\tfrac{\partial w''}{\partial x'}\right)^2,\quad \varepsilon_{y'}=\tfrac{\partial w''}{\partial y'}-\tfrac{w''}{R}\cos\varphi+\tfrac{1}{2}\left(\tfrac{\partial w''}{\partial y'}\right)^2\\ &\gamma_{x'y'}=\tfrac{\partial u''}{\partial y'}+\tfrac{\partial v''}{\partial x'}-2\tfrac{w''}{R}\sin\varphi\cos\varphi+\tfrac{\partial w''}{\partial x'}\tfrac{\partial w''}{\partial y'},\\ &k_{x'}=\tfrac{\partial^2 w''}{\partial x'^2},\quad k_{y'}=\tfrac{\partial^2 w''}{\partial y'^2},\quad k_{x'y'}=2\tfrac{\partial^2 w''}{\partial x'\partial y'}\end{aligned} \tag{16}$$

The physical equation of delaminations ($h_f \leqslant |z| \leqslant h_b$) in the local coordinate axes ($x' - y'$) is expressed as

$$\{\sigma\}_m = [\bar{Q}]_m(\{\varepsilon\}_m - \{\bar{\alpha}\}_m \Delta T_m - \{\bar{\bar{d}}\}_m E_z) \tag{17}$$

$$\{\bar{\varepsilon}\}_m = \{\, \varepsilon_{x'} \quad \varepsilon_{y'} \quad \gamma_{x'y'} \,\}^T - z_m \{\, k_{x'} \quad k_{y'} \quad k_{x'y'} \,\}^T, \quad (1 \leqslant m \leqslant J) \tag{18}$$

where the bias axial thermal expansion coefficient $\{\bar{\alpha}\}_m$, the bias axial piezoelectric coefficient $\{\bar{\bar{d}}\}_m$ and the bias axial stiffness $[\bar{Q}]_m$ of the mth layer in the local coordinate system are, respectively, shown as

$$\begin{aligned} &\{\bar{\alpha}\}_m = [T(\psi_m)]_\varepsilon \{\alpha\}_m, \quad \{\bar{\bar{d}}\}_m = [T(\psi_m)]_\varepsilon \{d\}_m, \\ &[\bar{\bar{Q}}]_m = [T(\psi_m)]_\sigma [Q]_m [T(\psi_m)]_\sigma^T \end{aligned} \tag{19}$$

where the transformation matrices $[T(\psi_m)]_\sigma$ and $[T(\psi_m)]_\varepsilon$ of stress and strain are the same as those in Eq. (13c), and $\psi_m = \varphi - \theta_m$ expresses the angle between the local coordinate axis ($x' - y'$) and the material's main axis (1–2) of the mth layer.

Utilizing Eqs. (17) and (18), the elastic energy of the mth layer's in delaminated sub-shells based on the local coordinate system is given by

$$U_m = \frac{1}{2} \int\int\int_{V_m} \left(\{\bar{\varepsilon}\}_m^T \{\bar{\sigma}\}_m \right) dV_m \tag{20}$$

The total elastic energy of delaminations is written as

$$\begin{aligned} U_{sub} = \sum_{m=1}^{J} U_m = &\tfrac{1}{2} \int\int_s \left(\{\bar{\varepsilon}_0\}^T [\bar{A}^s] \{\bar{\varepsilon}_0\} - 2\{\bar{\varepsilon}_0\}^T [\bar{B}^s] \{\bar{k}\} + \{\bar{k}\}^T [\bar{D}^s] \{\bar{k}\} \right) dS \\ &- \tfrac{1}{2} \int\int_S \left(\{\bar{\varepsilon}_0\}^T (\{\bar{N}^T\} + \{\bar{N}^E\}) - \{\bar{k}\}^T (\{\bar{M}^T\} + \{\bar{M}^E\}) \right) dS \end{aligned} \tag{21}$$

where $[\bar{A}^s], [\bar{B}^s]$ and $[\bar{D}^s]$ represent, respectively, the tension stiffness, the coupling tension-bending stiffness and the bending stiffness of delaminations in the local coordinate system, which are detailedly expressed in Appendix A.

In Eq. (21), $\{\bar{N}^T\}, \{\bar{M}^T\}, \{\bar{N}^E\}$ and $\{\bar{M}^E\}$ represent, respectively, the thermal force, the thermal moment, the electric force and the electric moment in the mid-plane of delaminations, and are given in Appendix A.

Only considering the polarization effect in the z direction of piezoelectric layers, the electric potential energy in the nth piezoelectric layer in delaminations in the local coordinate system is shown as

$$U_{En} = \frac{1}{2} \int\int\int_{V_n} \{E\}^T \{\bar{D}\}_n dV_n \tag{22}$$

When the number of piezoelectric layer of delaminations is $J1$, the total electric potential energy of the delaminations is written as

$$U_E = \sum_{n=1}^{J1} U_{En} \tag{23}$$

3. Critical loading and delaminated expansion

Here, the transverse and lateral displacements u'', v'' *and* w'' in the mid-plane deformation of delaminations are considered in computing the strain energy of delaminations. Because the thickness h_b of FGM laminated piezoelectric composite shells is much larger than the thickness h_s of delaminations, the connecting model between locally delaminations and FGM laminated piezoelectric composite shells is considered as fixed connection. Thus, the corresponding edge conditions of delaminations in the local coordinate system ($o'x'y'$) are written as

$$\begin{aligned} &u''|_\Gamma = u', \quad v'|_\Gamma = v'', \quad w''|_\Gamma = w', \quad \left.\frac{\partial w''}{\partial x'}\right|_\Gamma = \left.\frac{\partial w''}{\partial y'}\right|_\Gamma \\ &= 0, \text{ on the edge } \Gamma \end{aligned} \tag{24}$$

From Eqs. (15) and (24), a non-linear buckling model of elliptic delaminations satisfying the boundary conditions (24) is written as

$$\begin{aligned} u'' &= [x' \cos^2\varphi + (b_3 x' - y') \sin\varphi\cos\varphi - b_3 y' \sin^2\varphi]\varepsilon_0 \\ &+ (\cos\varphi + b_3 \sin\varphi) l_0 \varepsilon_0 + l_0 b_4 \sin\varphi + x' b_4 \sin\varphi\cos\varphi \\ &- y' b_4 \sin^2\varphi + (1 - x'^2/a^2 - y'^2/b^2)(a_0 x' + a_1 y') \\ v'' &= [b_3 x' \cos^2\varphi - (b_3 y' + x') \sin\varphi\cos\varphi + y' \sin^2\varphi]\varepsilon_0 \\ &+ (b_3 \cos\varphi - \sin\varphi) l_0 \varepsilon_0 + l_0 b_4 \cos\varphi + x' b_4 \cos^2\varphi \\ &- y' b_4 \sin\varphi\cos\varphi + (1 - x'^2/a^2 - y'^2/b^2)(a_2 x' + a_3 y') \\ w'' &= -R b_1 \varepsilon_0 - R b_2 + \left(1 - \frac{x'^2}{a^2} - \frac{y'^2}{b^2}\right)^2 (a_4 + a_5 x'^2 + a_6 y'^2 + a_7 x' y') \end{aligned} \tag{25}$$

where $a = \{\, a_0 \quad a_1 \quad a_2 \quad a_3 \quad a_4 \quad a_5 \quad a_6 \quad a_7 \,\}^T$ is called as a general coordinate representing the displacement coefficients of non-linealy buckling model for local delaminations.

Due to the transverse loading exerted on local delaminations is equal to zero and the boundary displacement of local delaminations is a given value, from Eqs. (21) and (23) the total potential energy of the local delaminations is expressed as

$$\begin{aligned} \Pi &= U_{sub} - U_E \\ &= \Pi\{u''(x', y', a_i), v''(x', y', a_i), w''(x', y', a_i), \varepsilon_0, E_z, \Delta T\} \end{aligned} \tag{26}$$

Applying variational principle for Eq. (26), yields

$$\left| \frac{\partial \Pi}{\partial a_i \partial a_j} \right| = 0, \ i,j = 0, 1, 2 \ldots 7 \tag{27}$$

The eigen-equation of Eq. (27) is expressed as

$$|[C1] + \varepsilon_{cr}[C2]| = 0 \tag{28}$$

where $[C1]$ and $[C2]$ are matrices related to the geometrical sizes, material properties and stacking sequences of FGM laminated piezoelectric composite shells and local delaminations. Substituting Eq. 25 into Eq. 16 and utilizing Eqs. (17)–(28), the corresponding eigenvalue ($\varepsilon_0 = \varepsilon_{cr}$) in Eq. (28) can be easily obtained. From the corresponding solutions ε_{cr} of eigenvalue equation (28), the smallest absolute value is expressed as the locally critical loading.

Here, the delaminated expansion following locally delaminated buckling is investigated. It is certain that the expanding direction of elliptical delamination is dependent on various factors. However, using an analytical method exactly describes the arbitrary shape change of local delaminations near the surface of laminated shells is difficult and is not reported so far. The main object of this paper is to give possibly expanding direction along two main axis of an initial elliptical delamination by comparing the values between the expanding forces G^b and G^a along the short and length axes of the elliptical delamination, so that an initial elliptical delamination can be predicted to evolve into a stable likely circular delamination or a likely slender crack. Therefore the result can be used to a useful reference to various numerical methods for solving the expansion of local delaminations of laminated structures.

Assuming that the requiring energy to produce a new delaminated interface is G_Γ which is generally obtained by experiment, the local delaminations will expand when the energy release rate G of the local delaminations satisfies $G \geqslant G_\Gamma$, in which G is expressed as

$$G = -\frac{dU_{sub}}{dS} + G_c \tag{29}$$

where U_{sub} is the strain energy of local delaminations, $S(=\pi ab)$ is an elliptically delaminated area, and G_c is the thin-film strain energy of local delaminations. Because the boundary of local delaminations near the surface of laminated shells is close and the local delaminations propagate in plane, the mixed effect of only crack propagation modes I and II is considered in the expression of the thin-film strain energy of local delaminations, as follows (Chai and Babcock, 1985):

$$G_c = \frac{\bar{A}^s_{22}\varepsilon_0^2}{2f_1}((\bar{A}^s_{12})^2 f_2 - 2A_{12}\bar{A}^s_{12} + 1) \tag{30}$$

where $f_1 = 1 - (\bar{A}^s_{12})^2$, $f_2 = \bar{A}^s_{11}/\bar{A}^s_{22}$, $\bar{A}^s_{11}, \bar{A}^s_{22}$ and $\bar{A}^s_{12}$ are the tension and shear stiffness coefficients of local delaminations in the local coordinate system, A_{12} is the shear stiffness coefficient of FGM laminated piezoelectric shells and h_s is the thickness of local delaminations.

The variations of U_{sub} and S give

$$dU_{sub} = \frac{\partial U_{sub}}{\partial a}da + \frac{\partial U_{sub}}{\partial b}db, \quad dS = \pi(adb + bda) \tag{31}$$

Substituting Eq. (31) into Eq. (29) yields

$$G = \left(G^a + G^b\frac{a}{b}\frac{db}{da}\right)\Big/\left(1 + \frac{a}{b}\frac{db}{da}\right) \tag{32}$$

$$G^a = \frac{-1}{\pi b}\frac{\partial U_{sub}}{\partial a} + G_c, \quad G^b = \frac{-1}{\pi a}\frac{\partial U_{sub}}{\partial b} + G_c \tag{33}$$

where G^a and G^b represent the expanding force of local laminations along the length axis and short axes of elliptical delaminations. Substituting Eqs. (21) and (30) into Eq. (33), the expanding forces G^a and G^b of local delaminations under electrical and thermal loads can be obtained, in which the bigger one represents the possibly expanding direction of the local delaminations.

4. Examples and discussions

In examples, the FGM laminated piezoelectric composite shells are made from FGM layer, fiber reinforced layers and piezoelectric layers, in which material properties are, respectively, expressed as

1. FGM layer:

$E_{Al} = 70$ GPa, $E_{Ce} = 151$ GPa, $\mu_{Al} = 0.3$, $\mu_{Ce} = 0.3$, $h_f = 10$ mm;

2. Carbon fiber reinforced layer:

$E_1 = 138(1 - \beta_1\Delta T)$ GPa, $E_2 = 8.96(1 - \beta_2\Delta T)$ GPa,
$G_{12} = 7.1(1 - \beta_2\Delta T)$ GPa

$\alpha_1 = -0.3(1 + \beta_1\Delta T)10^{-6}/^\circ$C, $\alpha_2 = 28.1(1 + \beta_1\Delta T)10^{-6}/^\circ$C,
$h_c = 0.5$ mm

3. Piezoelectric layer:

$E_i = 63(1 - \beta_1\Delta T)$ GPa, $G_{12} = 24.6(1 - \beta_1\Delta T)$ GPa,
$\alpha_i = 0.9(1 + \beta_1\Delta T)10^{-6}/^\circ$C,

$d_i = 2.54(1 + \beta_1\Delta T)10^{-10}$ m/V, $p_j = 20.(1 + \beta_1\Delta T)10^{-6}$ C/m^2 $^\circ$C,

$Q_j = 15.3(1 + \beta_1\Delta T)$ nF/m, $(i = 1, 2)$ and $(j = 1, 2, 3)$,
$h_p = 0.5$ mm

where the material's properties of carbon fiber reinforced layer and piezoelectric layer are taken as linear functions of temperature change, and the ratio coefficients is considered as $\beta_1 = 0.5 \times 10^{-3}/^\circ$C and $\beta_2 = 0.2 \times 10^{-3}/^\circ$C.

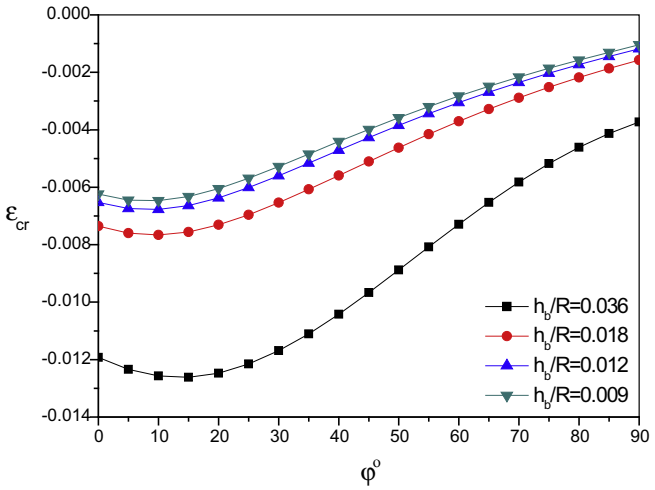

Fig. 3. Critical axial strain for local surface elliptical denomination [P_0] in FGM laminated piezoelectric composite shells [P_0/30°/60°/90°/FGM/90°/60°/30°/P_0] under radial electric field E_z and thermal loading ΔT, where $\Phi = 1$, $\Delta T_i = 50$ °C, $\Delta T_o = 200$ °C and $E_z = 2e6$ (V/m).

The temperature distribution along the thickness of FGM piezoelectric composite shells is nonlinear change as shown in Fig. 2. Because the thickness of piezoelectric composite layers is much smaller than that of functionally graded layer, only the thermal conduction effect of functionally graded layer is considered in the thermal conduction model along the thickness of functionally graded piezoelectric composite shells, and the temperature change along the thickness of piezoelectric and fiber layers is assumed as uniform distribution which is approach to a practical fact.

Fig. 3 shows the characteristics of critically axial strain for elliptical delaminations [P_0] near the surface of FGM laminated piezoelectric composite shells [P_0/30°/60°/90°/FGM/90°/60°/30°/P_0] subjected to the radial electric field and thermal loading. It is seen from Fig. 3 that the effect of the geometrical angle φ of elliptical delaminations on the critical axial strain of local buckling for the delaminations is dependent on the ratio of thickness to radius of FGM laminated piezoelectric composite shells. The critically axial strain varies as the geometric angle φ of local delaminations near the surface of FGM laminated piezoelectric composite shells with

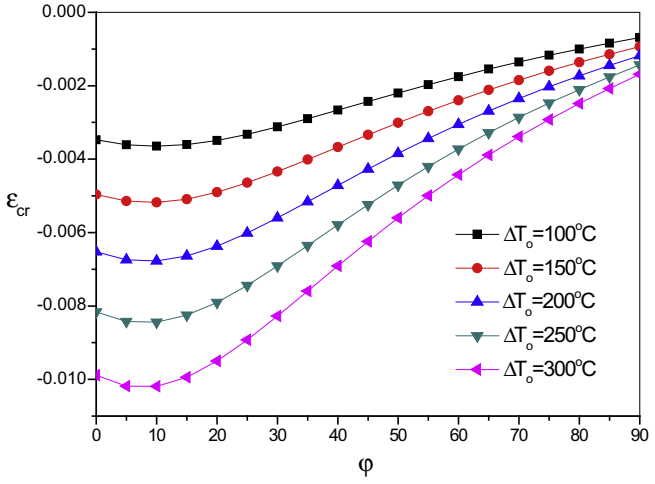

Fig. 4. Effect of thermal loading ΔT on the critical axial strain for local surface elliptical denomination [P_0] in FGM laminated piezoelectric composite shells [P_0/30°/60°/90°/FGM/90°/60°/30°/P_0] under radial electric field E_z, where $\Phi = 1$, $\Delta T_i = 50$ °C, $E_z = 2e6$ (V/m) and $h_b/R = 0.012$.

the thickness to radius ratio $h_b/R = 0.036$ increases when the geometric angle φ of local delaminations is less than 15°, then the critically axial strain nonlinearly decreases as the geometric angle φ of local delaminations increases. The critically axial strain decreases as the thickness to radius ratio h_b/R decreases.

It is plotted in Fig. 4 that the effect of temperature changes in FGM laminated piezoelectric composite shells on the critical axial strain of locally elliptical delamination. The effect of temperature changes on the critical axial strain of locally elliptical delamination is dependent on the geometric angle φ of local delaminations and the thickness to radius ratio. When the geometric axis of local delaminations is consistent with the geometric axis of FGM laminated piezoelectric composite shells ($\varphi = 0$), the effect of temperature changes on the critical axial loading of locally elliptical delamination is the maximum, and the temperature effect on the critical axial loading is gradually decreases as the geometric angle φ of local delaminations increases.

It is seen from Fig. 5 that the effect of the geometric angle φ of delaminations on the critical axial strain of the delaminations is dependent on the pattern of delaminations and the thickness to radius ratio h_b/R of FGM laminated piezoelectric composite shells. When the geometric angle φ of local delaminations is consistent with the geometric axis of FGM laminated piezoelectric composite shells with the thickness to radius ratio $h_b/R = 0.036$, the critical axial strain for the delamination $[P_0]$ is much larger that for the delaminations $[P_0/30°]$, and the difference between results from two delamination patterns $[P_0]$ and $[P_0/30°]$ is gradually decrease as the geometric angle φ of the local delaminations increases. The critical axial strain for the delamination $[P_0]$ is less than that for the delaminations $[P_0/30°]$ when the geometric angle φ of local delaminations is larger than 75°.

It is seen from Fig. 6 that for the FGM laminated piezoelectric composite shells with the thickness to radius ratio $h_b/R = 0.009$, the critically axial strain for the local delamination $[P_0/30°]$ near the surface of FGM laminated piezoelectric composite shells $[P_0/30°/60°/90°/FGM/90°/60°/30°/P_0]$ approaches to that for the local delamination $[P_0/0°]$ near the surface of FGM laminated piezoelectric composite shells $[P_0/0°/45°/-45°/FGM/-45°/45°/0°/P_0]$. The critically axial strain for the local delamination $[P_0/30°]$ near the surface of FGM laminated piezoelectric composite shells $[P_0/30°/60°/90°/FGM/90°/60°/30°/P_0]$ with the thickness to radius ratio $h_b/R = 0.036$ is larger than that for the local delamination $[P_0/0°]$ near the surface of FGM laminated piezoelectric composite shells $[P_0/0°/45°/-45°/FGM/-45°/45°/0°/P_0]$ when the geometric angle φ of local delamination is larger than 10°.

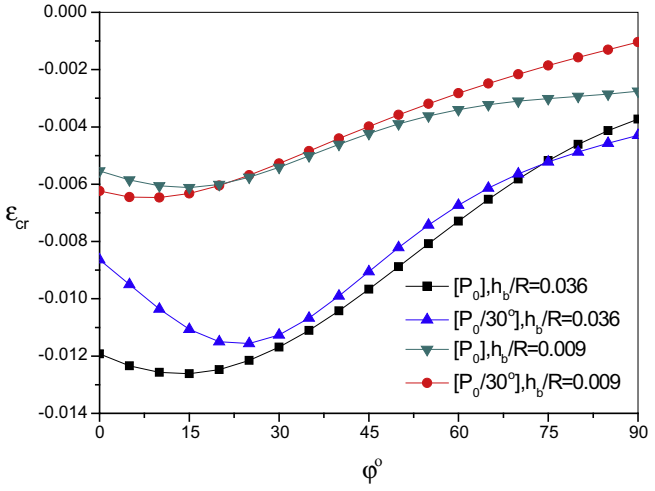

Fig. 5. Comparison of results from two elliptical denominations $[P_0]$ and $[P_0/30°]$ in FGM laminated piezoelectric composite shells $[P_0/30°/60°/90°/FGM/90°/60°/30°/P_0]$ under radial electric field E_z and thermal loadingΔT, where $\Phi = 1$, $\Delta T_i = 50$ °C, $\Delta T_o = 200$ °C and $E_z = 2e6$ (V/m).

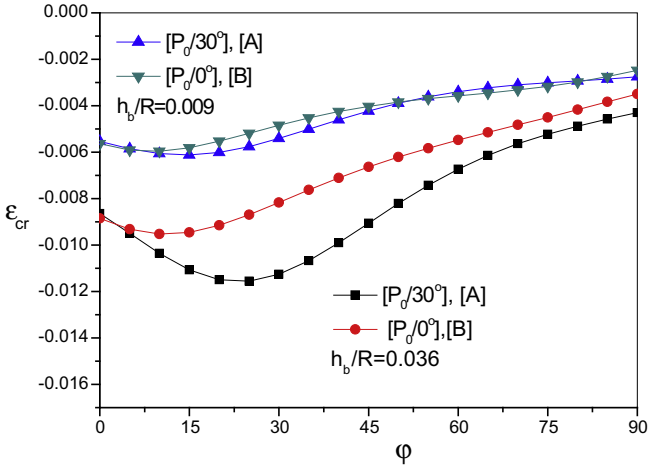

Fig. 6. Comparison of critical strains for denominations $[P_0/30°]$ and $[P_0/0°]$ in two laminated piezoelectric composite shells [A] and [B], where [A] = $[P_0/30°/60°/90°/FGM/90°/60°/30°/P_0]$, [B] = $[P_0/30°/60°/90°/FGM/90°/60°/30°/P_0]$, $\Phi = 1$, $\Delta T_i = 50$ °C, $\Delta T_o = 200$ °C and $E_z = 2e6$ (V/m).

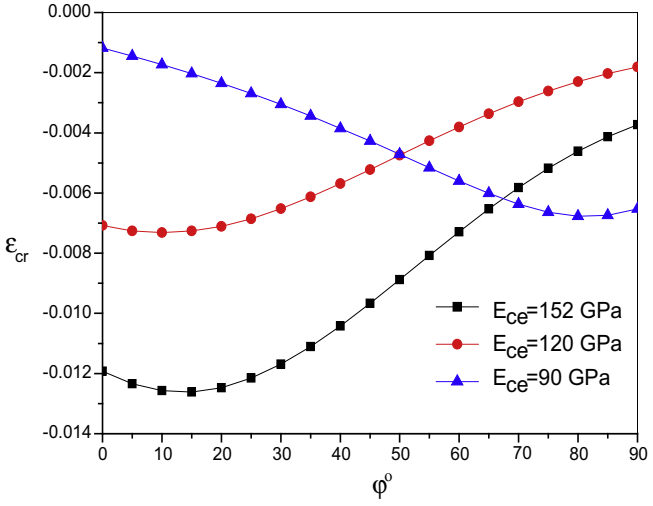

Fig. 7. The effect of FGM' property on critical axial loading for local elliptical denomination $[P_0]$ in FGM laminated piezoelectric composite shells $[P_0/30°/60°/90°/FGM/90°/60°/30°/P_0]$ under radial electric field E_z and thermal loading ΔT, where, $h_b/R = 0.036$, $\Phi = 1$, $\Delta T_i = 50$ °C, $\Delta T_o = 200$ °C and $E_z = 2e6$ (V/m).

Fig. 7 shows that the soft FGM material makes the critical loading for locally delamination near the surface of functionally graded laminated piezoelectric composite shells decrease when other parameters are fixed. When the stiffness of FGM layer decreases about percent forty, the effect of FGM layer on locally delaminated buckling is much smaller than that of piezoelectric composite layers. So that the critical loading for locally delamination is not only decrease, but also the distribution of the critical loading for locally delamination along the delamination angle appears in larger change.

Fig. 8 shows the distributions of expanding forces along the length and short axes of elliptical delaminations. The distribution of expanding forces along the length and short axes is dependent on the pattern of local delaminations. For the local delamination $[P_0]$, the expanding forces G^b along the short axis of elliptical delaminations are larger than the expanding forces G^a along the

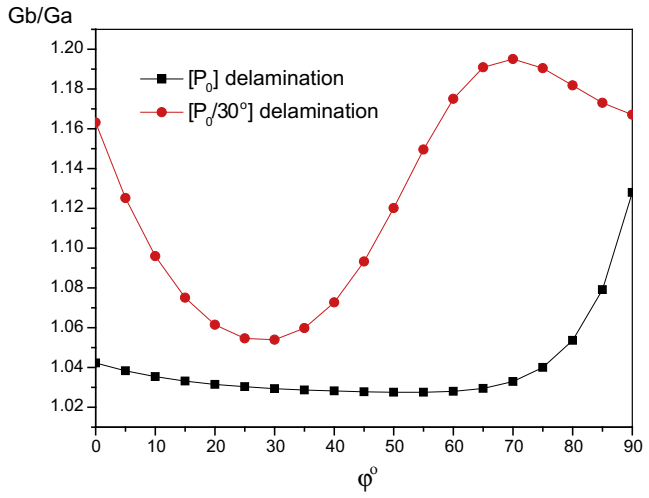

Fig. 8. The expanding forces G^a and G^b for local surface delamination are, respectively, along the length and short axis of elliptical delamination, where FGM laminated piezoelectric composite shells $[P_0/30°/60°/90°/FGM/90°/60°/30°/P_0]$, surface delamination $[P_0]$, $\Phi = 1$, $\Delta T_i = 50$ °C, $\Delta T_o = 200$ °C, ($E_z = 2e6$ (V/m) and $h_b/R = 0.012$.

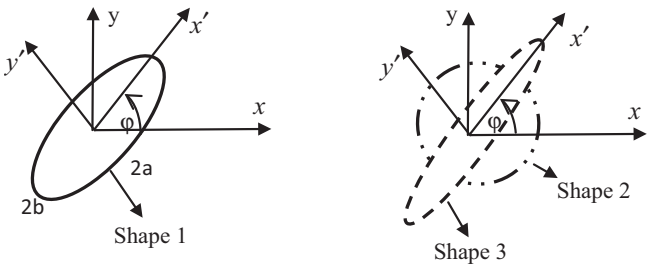

Fig. 9. Initial shape and possibly expanding shapes of local delamination, where shape 1 expresses an initial elliptical delamination, and shape 2 and shape 3 express a stable likely circular expanding shape or a likely slender crack, respectively.

length axis when the geometric angles φ of delamination are, respectively, 0°, 70° and 90°, where it is seen that the expanding direction of local delaminations will occur along the short axis of elliptical delaminations, so that the elliptical delaminations possibly expand into a stable circular delamination. For the local delaminations $[P_0/30°]$, the expanding force G^b along the short axis of elliptical delaminations approaches to the expanding force G^a along the length axis, and is independent on the geometric angles φ of delaminations, where the expanding direction of delaminations may occur either along the short axis or along the length axis of elliptical delaminations.

Considering that the mixed effect of only crack propagation modes I and II in the expression of the thin-film strain energy of local delaminations and comparing the values between the expanding forces G^b and G^a along the short and length axes of the elliptical delamination, an initial elliptical delamination can be predicted to evolve into a stable likely circular delamination or a likely slender crack as shown in Fig. 9.

Due to the report of study on locally buckling for elliptical delaminations near the surface of functionally graded laminated piezoelectric shells is a few in literatures, an accurate verification for the present method by using existed results is difficult. In order to give a verification example for the present method and solving process, a finite element model is utilized to simulate axial buckling for local elliptical delaminations near the surface of functionally graded laminated piezoelectric shells by means of Ansys program system, where calculation parameters are the same as those used in the present theoretical model. According to the theoretical analytical model as shown in Fig. 1, the graded change characteristics of FGM along the thickness is simulated by dividing the FGM layer into many thinner layers with the thickness same as the thickness of single fiber layer, where the material properties of each thinner layers are graded change along the thickness of FGM. The corresponding finite element model and net are simplified as shown in Fig. 10, in which quadratic quadrilateral layered shell elements (Shell-91) in Ansys program system are used for modeling different material layers of functionally graded laminated piezoelectric shells. The comparison of theoretical solution with finite element simulation is shown in Fig. 11. Because the contact characteristic of the interface layer between delaminated sub-shell

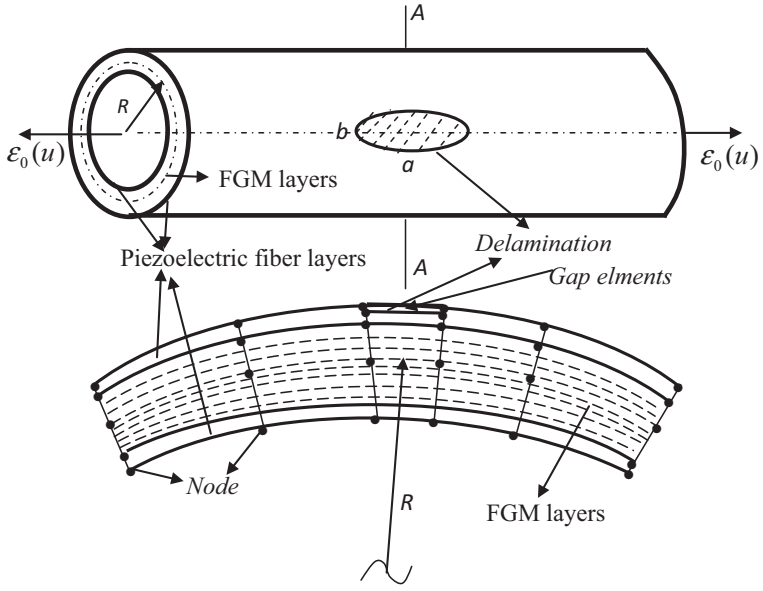

Fig. 10. The finite element model and net for calculating critical loading for local elliptical delamination near the surface of $[P_0/30°/60°/90°/FGM/90°/60°/30°/P_0]$ laminated piezoelectric composite shells.

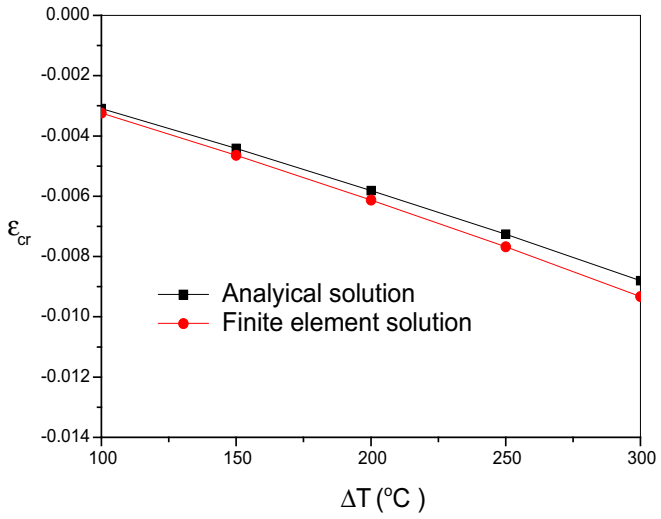

Fig. 11. Effect of thermal loading ΔT on the critical axial strain for local elliptical denomination $[P_0]$ near the surface of $[P_0/30°/60°/90°/FGM/90°/60°/30°/P_0]$ laminated piezoelectric composite shells, where $\Phi = 1$, $\Delta T_i = 50\ °C$, $E_z = 0$ and $h_b/R = 0.012$.

and laminated base-shell is considered in finite element simulation by using contact elements, the locally critical loading from the present theoretical solution without considering interface contact is lower than that from the finite element solution. It is seen from Fig. 11 that the maximum relative error between locally critical loads from two different modes is about 6%, thus a simple verification of the present theoretical work is given.

5. Conclusions

In this paper, an analytical method is presented to investigate nonlinear buckling for locally elliptical delaminations near the surface of FGM laminated piezoelectric composite shells under coupling thermal and electrical loads. Some main conclusions are given by

(1) The influence of the angle φ between the geometrical axis of elliptical delaminations and the geometrical axis of FGM laminated piezoelectric composite shells on the critical axial strain of local buckling for the elliptical delaminations is dependent on the thickness to radius ratio of FGM laminated piezoelectric composite shells.

(2) The effect of temperature changes on the critical axial strain of locally elliptical delamination appears in the maximum when the geometric axis of delaminations is consistent with the geometric axis of FGM laminated piezoelectric composite shells ($\varphi = 0$), and the effect of temperature change on the critical axial strain gradually decrease as the geometric angle φ of delaminations increases.

(3) The difference between critical axial strains obtained from two delaminated patterns $[P_0]$ and $[P_0/30°]$ is gradually decrease as the geometric angle φ of delaminations increases, and the critical axial strain for the local delamination $[P_0]$ is less than that for the delamination $[P_0/30°]$ when the geometric angle φ of local delaminations is larger than 75°.

(4) The influence of the stack sequences of FGM laminated piezoelectric composite shells on the critically axial strain for local delamination $[P_0]$ is dependent on the thickness to radius ratios of FGM laminated piezoelectric composite shells and the geometric angle φ of the local delamination.

(5) For the local delamination $[P_0]$, the expanding direction of delaminations will occur along the short axis of the elliptical delaminations, so that the elliptical delamination possibly evolves into a stable circular delamination. For the local delaminations $[P_0/30°]$, the expanding force G^b along the short axis of elliptical delamination approaches to the expanding force G^a along the length axis, thus to make the expanding direction of the local delamination occur in either the short axis or the length axis of elliptical delamination.

Acknowledgements

The authors wish to thank the National Science Foundation of China under No. 11172165.

Appendix A

$$[T(\theta_k)]_\sigma = \begin{bmatrix} \cos^2\theta_k & \sin^2\theta_k & -2\sin\theta_k\cos\theta_k \\ \sin^2\theta_k & \cos^2\theta_k & 2\sin\theta_k\cos\theta_k \\ \sin\theta_k\cos\theta_k & -\sin\theta_k\cos\theta_k & \cos^2\theta_k - \sin^2\theta_k \end{bmatrix} \tag{A-1}$$

$$[T(\theta_k)]_\varepsilon = \begin{bmatrix} \cos^2\theta_k & \sin^2\theta_k & -\sin\theta_k\cos\theta_k \\ \sin^2\theta_k & \cos^2\theta_k & \sin\theta_k\cos\theta_k \\ 2\sin\theta_k\cos\theta_k & -2\sin\theta_k\cos\theta_k & \cos^2\theta_k - \sin^2\theta_k \end{bmatrix} \tag{A-2}$$

$$[\bar{A}^s] = \sum_{m=1}^{J}[\bar{\bar{Q}}]_m(h_m - h_{m-1}), [\bar{B}^s] = \tfrac{1}{2}\sum_{m=1}^{J}[\bar{\bar{Q}}]_m(h_m^2 - h_{m-1}^2),$$
$$[\bar{D}^s] = \tfrac{1}{3}\sum_{m=1}^{J}[\bar{\bar{Q}}]_m(h_m^3 - h_{m-1}^3) \tag{A-3}$$

$$\{\bar{N}^T\} = \sum_{m=1}^{J}[\bar{\bar{Q}}]_m\{\bar{\bar{\alpha}}\}_m\Delta T(z_m - z_{m-1}), \quad [\bar{M}^T] = \tfrac{1}{2}\sum_{m=1}^{J}[\bar{\bar{Q}}]_m\{\bar{\bar{\alpha}}\}_m\Delta T(z_m^2 - z_{m-1}^2)$$
$$[\bar{N}^E] = \sum_{m=1}^{n}[\bar{\bar{Q}}]_m\{\bar{\bar{d}}\}_m E_z(z_m - z_{m-1}), \quad [\bar{M}^E] = \tfrac{1}{2}\sum_{m=1}^{J}[\bar{\bar{Q}}]_m\{\bar{\bar{d}}\}_m E_z(z_m^2 - z_{m-1}^2) \tag{A-4}$$

where J is the layer number of locally delaminated sub-shells.

References

Alashti, R.A., Khorasnd, M., 2011. Three-dimensional thermo-elastic analysis of a functionally graded cylindrical shell with piezoelectric layers by differential quadrature method. Int. J. Press. Vess. Pip. 88, 167–180.
Alibeigloo, A., 2010. Thermoelasticity analysis of functionally graded beam with integrated surface piezoelectric layers. Compos. Struct. 92, 1535–1543.
Alibeigloo, A., 2011. Thermoelastic solution for static deformations of functionally graded cylindrical shell bonded to thin piezoelectric layers. Compos. Struct. 93, 961–972.
Alibeigloo, A., Chen, W.Q., 2010. Elasticity solution for an FGMM cylindrical panel integrated with piezoelectric layers. Eur. J. Mech. A Solids 29, 714–723.
Bruno, D., Greco, F., 2000. An asymptotic analysis of delamination buckling and growth in layered plates. Int. J. Solids Struct. 37, 6239–6276.
Chai, H., Babcock, C.D., 1985. Two-dimensional modeling of compressive failure in delaminated laminates. J. Compos. Mater. 19, 67–98.
Chirica, I., Beznea, E.F., 2012. Buckling behavior of the multiple delaminated composite plates under shear and axial compression. Comput. Mater. Sci. 64, 173–178.
Craven, R., Iannucci, L., Olsson, R., 2010. Delamination buckling: a finite element study with realistic delamination shapes, multiple delaminations and fibre fracture cracks. Compos. Part A 41, 684–692.
Ghasemnejad, H., Furquan, A.S.M., Mason, P.J., 2010. Charpy impact damage behaviour of single and multi-delaminated hybrid composite beam structures. Mater. Des. 31, 3653–3660.

Kharazi, M., Ovesy, H.R., Taghizadeh, M., 2010. Buckling of the composite laminates containing through-the-width delaminations using different plate theories. Compos. Struct. 92, 1176–1183.
Li, D.H., 2012. Delamination buckling for composite laminated cylindrical shells in Hamilton system. Civ. Struct. Eng. 4, 222–230.
Malekzadeh, P., Heydarpour, Y., Golbahar Haghighi, M.R., Vaghefi, M., 2012. Transient response of rotating laminated functionally graded cylindrical shells in thermal environment. Int. J. Press. Vess. Pip. 98, 43–56.
Meng, F., Wang, H., Wang, X., Li, Z., 2010. Elliptically delaminated buckling near the surface of piezoelectric laminated shells under electric and thermal loads. Compos. Struct. 92, 684–690.
Naghipour, P., Bartsch, M., Voggenreiter, H., 2011. Simulation and experimental validation of mixed mode delamination in multidirectional CF/PEEK laminates under fatigue loading. Int. J. Solids Struct. 48, 1070–1081.
Obdržáleka, V., Vrbkab, J., 2011. On the applicability of simple shapes of delaminations in buckling analyses. Compos. Part B 42, 538–545.
Reddy, J.N., 2000. Analysis of functionally graded plates. Int. J. Numeric Methods Eng. 47, 663–684.
Ren, L., 2008. A theoretical study on shape control of arbitrary lay-up laminates using piezoelectric actuators. Compos. Struct. 83, 110–118.
Sarangi, S.K., Ray, M.C., 2013. Smart control of nonlinear vibrations of doubly curved functionally graded laminated composite shells under a thermal environment using 1–3 piezoelectric composites. Int. J. Mech. Mat. Des. 9, 253–280.
Shariyat, M., 2008. Dynamic buckling of suddenly loaded imperfect hybrid FGM cylindrical shells with temperature-dependent material properties under thermo-electro-mechanical loads. Int. J. Mech. Sci. 50, 1561–1571.
Shariyat, M., 2009a. Vibration and dynamic buckling control of imperfect hybrid FGM plates with temperature-dependent material properties subjected to thermo-electro-mechanical loading conditions. Compos. Struct. 88, 240–252.
Shariyat, M., 2009b. Dynamic buckling of imperfect laminated plates with piezoelectric sensors and actuators subjected to thermo-electro-mechanical loadings, considering the temperature-dependency of the material properties. Compos. Struct. 88, 228–239.
Shen, H.S., 2005. Postbuckling of axially loaded FGM hybrid cylindrical shells in thermal environments. Compos. Sci. Technol. 65, 1675–1690.
Shen, H.S., 2009. A compassion of buckling and postbuckling behavior of FGMM plates with piezoelectric fiber reinforced composite actuators. Compos. Struct. 91, 375–384.
Sheng, G.G., Wang, X., 2009a. Active control of functionally graded laminated cylindrical shells. Compos. Struct. 90, 448–457.
Sheng, G.G., Wang, X., 2009b. Studies on dynamic behavior of functionally graded cylindrical shells with PZT layers under moving loads. J. Sound Vib. 323, 772–789.
Sheng, G.G., Wang, X., 2010. Response and control of functionally graded laminated piezoelectric shells under thermal shock and moving loadings. Compos. Struct. 93, 132–141.
Sheng, G.G., Wang, X., 2011. Non-linear response of functionally graded cylindrical shells under mechanical and thermal loads. J. Therm. Stresses 34, 1105–1118.
Tay, T.E., 2003. Characterization and analysis of delamination fracture in composites: an overview of developments. Appl. Mech. Rev. 56, 1–32.
Tsouvalis, N.G., Garganidis, G.S., 2011. Buckling strength parametric study of composite laminated plates with delaminations. Ships Offsh. Struct. 6, 93–104.
Wu, C.P., Syu, Y.S., 2007. Exact solutions of functionally graded piezoelectric shells under cylindrical bending. Int. J. Solids Struct. 44, 6450–6472.